A Fisher information analysis of joint localization and synchronization in near field

A Fisher Information Analysis of Joint Localization and Synchronization in Near Field

Henk Wymeersch
Department of Electrical Engineering
Chalmers University of Technology
e-mail: henkw@chalmers.se

***Abstract*—In 5G communication, arrays are used for both positioning and communication. As the arrays become larger, the far-field assumption is increasingly being violated and curvature of the wavefront should be taken into account. In this paper, we use a single large linear array and relative phase measurements to perform the localization and synchronization. We explicitly contrast near-field and far-field uplink localization performance in the presence of a clock bias from a Fisher information perspective and show how a simple algorithm can provide a coarse estimate of a user's location and clock bias.**

I. Introduction

Cellular localization has largely relied on measurements of time-difference-of-arrival in either uplink or downlink. Such measurements can cope with the clock bias of the user, but require multiple base stations (BSs) [1]. With 5G, where large arrays are used to provide improved spectral efficiency, angle measurements have become possible [2], [3]. Estimating the angle-of-arrival (AOA) at different BSs, the user's location is determined by a set of bearing lines, so that localization can be performed without any stringent synchronization requirements [4]. When both user and base station are equipped with large arrays, the user's position and orientation can be inferred [5]. Extensive studies have been performed to assess the fundamental performance of array-based positioning [6]–[8] (through the Cramér-Rao bound (CRB)), as well as to develop practical algorithms [5], [9]. All these works assume far-field propagation (plane wave assumption), where the user is far away from the BS. With communication systems beyond 5G targeting novel technological enablers, such as large intelligent surfaces and extreme aperture arrays [10], the far-field propagation condition may be violated, requiring us to revisit the models, performance characterization, and algorithm design. Such activities have now started in communication [11], [12] and radio localization [13] and are the main topic of this paper.

Near-field localization dates back around 30 years in the context of source localization. The early work [14] studied the impact of an imperfectly calibrated array on near-field source localization and a calibration method was proposed, while [15] estimated the direction-of-arrival (DOA) of multiple sources using the MUSIC algorithm and a maximum likelihood (ML) approach. The latter was shown to be superior in low SNR conditions, though comes at a significant complexity cost. In [16], an ESPRIT-based method was proposed and the performance was theoretically determined. In [17], a multi-source CRB was derived for stochastic sources, highlighting the benefits of centro-symmetric arrays. An overlapping sub-array approach was proposed in [18] for low complexity range and bearing estimation. In [19], time-varying sources were studied in the narrowband regime in terms of the CRB. Range and bearing estimation were also treated in [20], based on sparse recovery techniques. The localization of near- and far-field sources was proposed in [21]. A simplified CRB for near-field positioning was derived in [22], as well as an algorithm that directly exploits the wavefront curvature for positioning. In contrast to the above works in the narrowband regime, [23] considered spatial wideband signals (where signals arrive at different antenna elements with different resolvable delays) and derived the CRB and an ML estimator. The extension [24] relied on an expectation-maximization method, which is computationally less demanding than ML. Positioning using large intelligent surface was considered in [13], which showed that the CRB reduces quadratically in the size of the array. Most of these works rely on second-order statistics and are thus data-intensive.

In this paper, in contrast to the above works, we consider not only the position but also the clock bias of the transmitter to be unknown. This leads us to investigate joint localization and synchronization in near-field. Moreover, we do not rely on second-order statistics and instead exploit the communication signal directly. Our main contributions are: (i) a Fisher information analysis of uplink near-field joint localization and synchronization with a linear array; (ii) a simple joint localization and synchronization method using sub-array processing.

The remained of this paper is organized as follows: we first provide a general system model in II, followed by a Fisher information analysis of the conventional far-field case in Section III. Then follows our main contribution in Section IV: the Fisher information analysis of the near-field and spatial wideband cases. Numerical results are reported in Section V, followed by our conclusions.

II. System Model

We consider a 2D scenario with a single-antenna user equipment (UE) with unknown location $\mathbf{x} = [x, y]^{\mathrm{T}}$ (or $[d, \theta]^{\mathrm{T}}$ in polar coordinates, with $d = \|\mathbf{x}\|$ and $\theta = \arccos(x/\|\mathbf{x}\|)$) and a small BS (e.g., indoors in close proximity to the UE)

with an $N+1$-element[1] linear array with element spacing Δ, with locations $\mathbf{x}_n = [n\Delta, 0]^{\mathrm{T}}$, $n \in \{-N/2, \ldots, N/2\}$. The UE has an unknown clock bias B (expressed in meters) and sends a known OFDM signal with transmit power P_t at a high carrier frequency f_c (28 GHz or higher) and a total bandwidth $W = (K+1)\Delta_f$, where Δ_f is the subcarrier spacing and $K+1$ is the number of subcarriers. For notational convenience, but without any loss of generality, we let $k \in \{-K/2, \ldots, K/2\}$. We further introduce $d_n = \|\mathbf{x} - \mathbf{x}_n\|$ (so $d = d_0$) and $\delta_n = \|\mathbf{x} - \mathbf{x}_n\| - B$, which allows us to express the uplink signal observed on antenna n, subcarrier k:

$$y_n[k] = \alpha_n s[k] e^{-j\frac{2\pi}{\lambda}\xi_n[k]} + \sum_{l=1}^{L} \alpha_{n,l} s[k] e^{-j\frac{2\pi}{\lambda}\xi_{n,l}[k]} + w_n[k], \tag{1}$$

where $w_n[k]$ complex zero-mean Gaussian noise with variance $N_0/2$ per real dimension. Taking the phase at the center antenna ($N = 0$) and center subcarrier $k = 0$ as reference, i.e., $\xi_0[0] = 0$, the phase at any antenna n and any subcarrier k is given by

$$\xi_n[k] = (d_n - d_0) + k\frac{\delta_n}{(K+1)\,T_s f_c}, \tag{2}$$

in which $T_s = 1/W$. The first term is the $d_n - d_0$ is the difference in path length with respect to the center antenna, while the second term depends on the absolute delay δ_n, and grows with the subcarrier index.

Example 1. *The phase $-2\pi\xi_n[k]/\lambda$ is shown in Fig. 2, for $\Delta = \lambda/2$, where the left figure shows the evolution of the phase with n for various distances d_0 as a function of the antenna index n and the right figure the evolution of the phase as a function of the subcarrier index k, for different antenna elements. We see from Fig. 2 (left) that when d_0 is small, the phase exhibits a nonlinear behavior as a function of n, while Fig. 2 (right) illustrates that for small d_0, different antenna elements see different absolute delays δ_n (note that this effect is only visible when we have a large bandwidth W).*

The complex channel gain at antenna n is $\alpha_n = \rho_n e^{j\psi}$ with $\rho_n = \lambda/(2\pi d_n)$ and $\psi = -2\pi d_0/\lambda$. Similarly, $\alpha_{n,l}$ is the complex gain of non-line-of-sight (NLOS) path l, $\xi_{n,l}[k]$ is a phase increasing with k due to the delay of the NLOS path l. We will make several assumptions, in order to facilitate compact closed-form expressions: we assume that α_n is not used directly for localization (so it is treated as a separate unknown) [5], [25]; $|\alpha_n| \gg |\alpha_{n,l}|, \forall l$ so that the line-of-sight (LOS) path is dominant [11], [17], [19], [23] (the robustness of the proposed method to multipath will be evaluated in Section V-B); the transmitted signal spectrum is symmetric ($|s[k]| = |s[-k]|$). Our goal is to determine $\mathbf{x}$ and B from the observation $\mathbf{Y} \in \mathbb{C}^{(N+1)\times(K+1)}$, though the proposed methods can be combined with tracking as in [25] to account for user mobility and clock drift [26].

[1]The analysis can easily be modified for an array with N elements, with locations $\mathbf{x}_n = [\Delta/2 + n\Delta, 0]^{\mathrm{T}}$, for $n = -N/2, \ldots, N/2-1$.

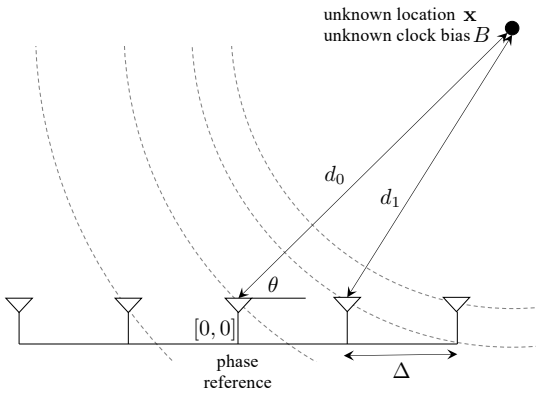

Fig. 1. Scenario with a transmitting source and a receiver array. In near-field, the phase across the antenna elements changes nonlinearly. In spatial wide-band, the delay across the antenna elements changes noticeably.

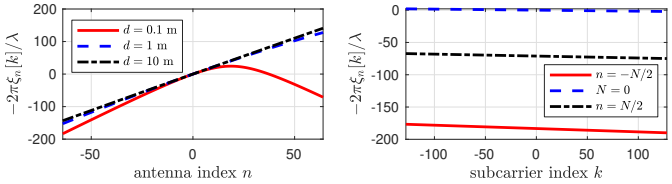

Fig. 2. Left: Plot of the signal phase $-2\pi\xi_n[k]/\lambda$ as a function of the antenna index n for different distances d between transmitter and the phase reference of the receiver. Right: Plot of the signal phase $-2\pi\xi_n[k]/\lambda$ as a function of the subcarrier index k for different antenna indices, for $d = 0.1$ m. Parameters: $K = 257$, $N = 129$, $f_c = 28$ GHz, $W = 1.4$ GHz, $\Delta = \lambda/2$.

Terminology: We distinguish the following operating conditions.

- *Far-field vs near-field:* When $\|\mathbf{x}\| > 2(N\Delta)^2/\lambda$, the far-field regime with plane wave assumption holds. When $0.62\sqrt{(N\Delta)^3/\lambda} < \|\mathbf{x}\| < 2(N\Delta)^2/\lambda$, we operate in the radiative near-field zone, where wavefront curvature is non-negligible [21].
- *Narrowband vs wideband:* When $W < c/(N\Delta)$, the signals at the different antennas are not resolvable in the delay domain and communication is narrowband. When $W > c/(N\Delta)$, we consider the signals to be spatially wideband in the sense that they are resolvable in the delay domain at different antennas [23].
- *Beam squint:* When $W > f_c/10$, the wavelength of the signal varies significantly over its bandwidth, leading to beam squint. Generally, beam squint implies spatial wideband operation, but not vice versa.

Throughout this paper, we assume that the bandwidth is sufficiently small to ignore beam squint (i.e., $W \ll f_c$).

III. Standard Far-Field and Narrowband Condition

A. Model and Fisher Information Matrix

In far-field and narrowband condition, the standard model reverts to [5], [15]

$$y_n[k] = \alpha_0 s[k] e^{-j\frac{2\pi}{\lambda}\xi_n[k]} + w_n[k], \tag{3}$$

where

$$\xi_n[k] = -n\Delta\cos\theta - k(d-B)r_f, \tag{4}$$

with $r_f = \Delta_f/f_c$. This model is derived by taking a first-order Taylor series expansion of $d_n - d_0$ around $n\Delta/d_0 = 0$ [15] in combination with $\delta_n \approx \delta_0$ and $\alpha_n \approx \alpha_0$. The Fisher information matrix (FIM) of $\boldsymbol{\eta} = [\rho, \psi, d, \theta, B]^{\mathrm{T}}$ is composed of the sum of the FIM for each subcarrier and each antenna $\mathbf{J}^{\mathrm{S}}(\boldsymbol{\eta}) = \sum_{n=-N/2}^{N/2}\sum_{k=-K/2}^{K/2}\mathbf{J}_n[k]$ where [27]

$$\mathbf{J}_n[k] = \frac{1}{N_0}|s[k]|^2\Re\left\{\nabla_{\boldsymbol{\eta}}^{\mathrm{H}}(\alpha_0 e^{-j\frac{2\pi}{\lambda}\xi_n[k]})\nabla_{\boldsymbol{\eta}}(\alpha_0 e^{-j\frac{2\pi}{\lambda}\xi_n[k]})\right\} \tag{5}$$

in which the derivatives are given by

$$\nabla_{\boldsymbol{\eta}}^{\mathrm{T}}(\alpha_0 e^{-j\frac{2\pi}{\lambda}\xi_n[k]}) = e^{-j\frac{2\pi}{\lambda}\xi_n[k]}\begin{bmatrix} e^{j\psi} \\ j\alpha_0 \\ -j\frac{2\pi}{\lambda}\alpha_0\frac{\partial\xi_n[k]}{\partial d} \\ -j\frac{2\pi}{\lambda}\alpha_0\frac{\partial\xi_n[k]}{\partial\theta} \\ -j\frac{2\pi}{\lambda}\alpha_0\frac{\partial\xi_n[k]}{\partial B}\end{bmatrix}, \tag{6}$$

where $\partial\xi_n[k]/\partial d = -kr_f$, $\partial\xi_n[k]/\partial\theta = n\Delta\sin\theta$, $\partial\xi_n[k]/\partial B = kr_f$. We find that, since $\Re\{j\} = 0$, $J_{1,i\neq 1} = 0$ (here $J_{i,i'}$ refers the entry in $\mathbf{J}(\boldsymbol{\eta})$ on row i, column i'). Hence, we can ignore ρ when determining the FIM of $\boldsymbol{\eta} = [\psi, d, \theta, B]^{\mathrm{T}}$. We introduce $\mathbf{e}_i$ as an all-zero vector with a 1 on index i, $\mathbf{b} = [0, 1, 0, -1]^{\mathrm{T}}$, and $\gamma = |\alpha_0|^2(2\pi/\lambda)^2/N_0$. Then

$$\mathbf{J}^{\mathrm{S}}(\boldsymbol{\eta}) = \gamma\mathbf{J}_1^{\mathrm{S}} + \gamma\mathbf{J}_2^{\mathrm{S}} + \gamma\mathbf{J}_3^{\mathrm{S}}, \tag{7}$$

where

$$\mathbf{J}_1^{\mathrm{S}} = \left(\frac{\lambda}{2\pi}\right)^2 E_{K,0}E_{N,0}\mathbf{e}_1\mathbf{e}_1^{\mathrm{T}} \tag{8}$$

$$\mathbf{J}_2^{\mathrm{S}} = E_{K,2}E_{N,0}r_f^2\mathbf{b}\mathbf{b}^{\mathrm{T}} \tag{9}$$

$$\mathbf{J}_3^{\mathrm{S}} = E_{K,0}E_{N,2}\Delta^2\sin^2\theta\,\mathbf{e}_3\mathbf{e}_3^{\mathrm{T}}, \tag{10}$$

in which $E_{K,i} = \sum_{k=-K/2}^{K/2}k^i|s[k]|^2$ and $E_{N,i} = \sum_{n=-N/2}^{N/2}n^i$. The directions in which we obtain information are *radially* (along the line from the center of the BS array to the UE) and *tangentially* (orthogonal to the line between BS array center and UE). Transformation to the position domain is achieved as follows. With $x = d\cos\theta$ and $y = d\sin\theta$, the FIM of $\mathbf{J}(\mathbf{x}, B)$ is given by $\mathbf{J}(\psi, \mathbf{x}, B) = \mathbf{T}^{\mathrm{T}}\mathbf{J}(\boldsymbol{\eta})\mathbf{T}$ with Jacobian given by

$$\mathbf{T} = \begin{bmatrix} 1 & 0 & 0 & 0 \\ 0 & x/d & y/d & 0 \\ 0 & -y/d^2 & x/d^2 & 0 \\ 0 & 0 & 0 & 1\end{bmatrix}. \tag{11}$$

Since ψ does not depend on the other parameters,

$$\mathbf{J}(\mathbf{x}, B) = \gamma E_{K,2}E_{N,0}r_f^2\mathbf{e}_{\mathbf{x}}\mathbf{e}_{\mathbf{x}}^{\mathrm{T}} + \gamma E_{K,0}E_{N,2}\Delta^2y^2\frac{1}{\|\mathbf{x}\|^4}\mathbf{e}_{\mathbf{x},\perp}\mathbf{e}_{\mathbf{x},\perp}^{\mathrm{T}}. \tag{12}$$

where $\mathbf{e}_{\mathbf{x}} = [x/d,\, y/d,\, 1]^{\mathrm{T}}$ and $\mathbf{e}_{\mathbf{x},\perp} = [-y/d,\, x/d,\, 0]^{\mathrm{T}}$. Since $\mathbf{e}_{\mathbf{x}}$ is orthogonal to $\mathbf{e}_{\mathbf{x},\perp}$, this decomposition shows that delay estimation provides radial information with intensity $\gamma E_{K,2}E_{N,0}r_f^2$ and AOA estimation provides tangential information with location-dependent intensity $\gamma E_{K,0}E_{N,2}\Delta^2y^2/\|\mathbf{x}\|^4$. Hence, AOA information is only useful for short distances. Moreover, the matrix $\mathbf{J}(\mathbf{x}, B)$ is rank 2, so B and $\mathbf{x}$ are not jointly identifiable.

B. Localization Algorithm

We organize the observations $y_n[k]$ in a $(N+1)\times(K+1)$ matrix:

$$\mathbf{Y} = \alpha_0\,\mathbf{a}_{N+1}(\cos\theta)\mathbf{a}_{K+1}^{\mathrm{H}}(\delta_0 r_f)\mathbf{S} + \mathbf{W} \tag{13}$$

where $\mathbf{S}$ is a diagonal matrix containing the $K+1$ pilot symbols and $\mathbf{a}_{M+1}(\cdot)$ is a vector of length $M+1$ with entries $[\mathbf{a}_{M+1}(\beta)]_m = \exp\left(j2\pi\beta m/(M+1)\right)$, for $m = -M/2, \ldots, M/2$. Similar to [5], we exploit the sparse nature of $\mathbf{Y}$ by applying a 2D-FFT

$$\mathbf{Z} = \mathbf{F}_{N+1}\mathbf{Y}\mathbf{S}^{\mathrm{H}}(\mathbf{S}\mathbf{S}^{\mathrm{H}})^{-1}\mathbf{F}_{K+1} \tag{14}$$

to the observation $\mathbf{Y}\mathbf{S}^{\mathrm{H}}(\mathbf{S}\mathbf{S}^{\mathrm{H}})^{-1}$, where the impact of the pilot symbols has been removed. This also allows multiple users to be treated independently if there is no pilot contamination [28]. Here, $\mathbf{F}_M$ denotes the $M\times M$ discrete Fourier transform matrix. Higher accuracy can be achieved by zero-padding $\mathbf{Y}$ and applying larger FFT matrices. The peak of $|\mathbf{Z}|$ directly provides us an estimate of $\cos\theta$ and $\delta_0 r_f$, which can directly be converted to the UE position in polar coordinates. As indicated by the FIM, the parameters are not identifiable, so we can only localize the user when the bias B is known. The complexity of this method is of order $\mathcal{O}(NK\log KN)$.

IV. Near-Field and Spatial Wideband Conditions

A. Narrowband Near-field Model and FIM

When signals arriving at different antennas are not resolvable in delay, the model (1) applies with (2) specialized to

$$\xi_n[k] = d_n + (kr_f - 1)d - kr_fB. \tag{15}$$

We can now state the following result.

Theorem 1. *In the case of narrowband near-field operation, the FIM of the parameter $\boldsymbol{\eta} = [\psi, d, \theta, B]^T$ is*

$$\mathbf{J}^N(\boldsymbol{\eta}) = \gamma\frac{A_0^{(0)}}{E_{N,0}}\mathbf{J}_1^S + \gamma\frac{A_0^{(0)}}{E_{N,0}}\mathbf{J}_2^S + \gamma\frac{A_2^{(2)}}{E_{N,2}}\mathbf{J}_3^S + \gamma\mathbf{J}_4^N + \gamma\mathbf{J}_5^N,$$

where $A_i^{(j)} = \sum_n (d/d_n)^{j+2}\,n^{-i}$ and

$$\mathbf{J}_4^N = \frac{\lambda}{2\pi}E_{K,0}\begin{bmatrix} 0 & \mathbf{j}^T \\ \mathbf{j} & \mathbf{0}_{3\times 3}\end{bmatrix}$$

$$\mathbf{J}_5^N = E_{K,0}\begin{bmatrix} 0 & \mathbf{0}^T & 0 \\ \mathbf{0} & \mathbf{C} & \mathbf{0} \\ 0 & \mathbf{0}^T & 0\end{bmatrix}$$

with $\mathbf{j} = [-\frac{\Delta}{d}\cos\theta A_1^{(1)} + A_0^{(1)} - A_0^{(0)},\, A_1^{(1)}\Delta\sin\theta,\, 0]^T$, $C_{1,1} = A_0^{(0)} + A_0^{(2)} - 2(\frac{\Delta}{d}\cos\theta A_1^{(2)} + A_0^{(1)} - \frac{\Delta}{d}\cos\theta A_1^{(1)}) + \frac{\Delta^2}{d^2}A_2^{(2)}\cos^2\theta$, $C_{1,2} = C_{2,1} = \Delta\sin\theta A_1^{(2)} - \Delta\sin\theta A_1^{(1)}$, $C_{2,2} = 0$.

Proof. We readily find that $\partial\xi_n[k]/\partial d = (d - n\Delta\cos\theta)/d_n - 1 + kr_f$, $\partial\xi_n[k]/\partial\theta = dn\Delta\sin\theta/d_n$, $\partial\xi_n[k]/\partial B = -kr_f$. Substituting these derivatives in (6) and then in (5), followed by applying the Jacobian, we obtain the desired result. □

We observe that the first 3 components are similar to those in the standard case (7), up to a scaling. On the other hand, $\mathbf{J}_4^{\mathrm{N}}$ and $\mathbf{J}_5^{\mathrm{N}}$ are due to the near-field propagation. In particular, $\mathbf{J}_4^{\mathrm{N}}$ couples the channel phase ψ with the UE distance d and the AOA θ. The diagonal element $C_{1,1}$ in $\mathbf{J}_5^{\mathrm{N}}$ provides additional information on the distance, which allows $\mathbf{J}^{\mathrm{N}}(\boldsymbol{\eta})$ to become full rank. This information is due to the dependence of the curvature on the UE location, but not on the bias.

B. Spatial Wideband Far-field Model and FIM

Under spatial wideband far-field communication, the model (1) applies with (2) specialized to

$$\xi_n[k] = -n\Delta\cos\theta + k(d_n - B)r_f. \tag{16}$$

We can then state the following result.

Theorem 2. *In the case of spatial wideband far-field operation, the FIM of the parameter $\boldsymbol{\eta} = [\psi, d, \theta, B]^T$ is*

$$\mathbf{J}^W(\boldsymbol{\eta}) = \gamma\frac{A_0^{(0)}}{E_{N,0}}\mathbf{J}_1^S + \gamma\mathbf{J}_2^W + \gamma\frac{A_2^{(2)}}{E_{N,2}}\mathbf{J}_3^S + \gamma\mathbf{J}_4^W,$$

where

$$\mathbf{J}_2^W = E_{K,2}r_f^2\begin{bmatrix} 0 & 0 & 0 & 0 \\ 0 & A_0^{(2)} & 0 & -A_0^{(1)} \\ 0 & 0 & 0 & 0 \\ 0 & -A_0^{(1)} & 0 & A_0^{(0)} \end{bmatrix}$$

$$\mathbf{J}_4^W = E_{K,2}r_f^2\frac{\Delta\cos\theta}{d}\begin{bmatrix} 0 & 0 & 0 & 0 \\ 0 & A_2^{(2)}\frac{\Delta}{d}\cos\theta - 2A_1^{(2)} & 0 & A_1^{(1)} \\ 0 & 0 & 0 & 0 \\ 0 & A_1^{(1)} & 0 & 0 \end{bmatrix}$$

Proof. We readily find that $\partial\xi_n[k]/\partial d = kr_f(d - n\Delta\cos\theta)/d_n$, $\partial\xi_n[k]/\partial\theta = n\Delta\sin\theta$, $\partial\xi_n[k]/\partial B = -kr_f$. Substituting these derivatives in (6) and then in (5), followed by applying the Jacobian, we obtain the desired result. □

We observe that the radial information in $\mathbf{J}_2^{\mathrm{W}}$ is now scaled and that there is an additional term $\mathbf{J}_4^{\mathrm{W}}$ that provides distance information with positive information $E_{K,2}r_f^2A_2^{(2)}\Delta^2\cos^2\theta/d^2$, which is important for large Δ/d. The information is larger near the end-fire ($\theta \approx 0$), as this is where the delay spread is maximized. Note that the amount of information due to large bandwidth is generally less than the amount of information due to near-field.

C. Localization and Synchronization Algorithm

From the Fisher information analysis, we find that for small Δ (e.g., $\Delta = \lambda/2$) the amount of information increase due to near-field is more pronounced than due to spatial wideband. This is also confirmed by Fig. 2, where the nonlinear curvature of the phase across antennas (left Figure) is more significant than the difference in slope for different antennas (right Figure). Based on this finding, we focus on the near-field case.

Algorithm 1 Sub-array Localization and Synchronization

procedure LOCALIZE-NEAR-FIELD($\mathbf{Y}$)
  Determine $\tilde{N} \in \mathbb{N}_{\geq 1}$:
$$\tilde{N} \leq \sqrt{\bar{d}\lambda}/(2\Delta^2) \quad \text{and} \quad \tilde{N} \ll c/(W\Delta)$$
  Partition rows of $\mathbf{Y}$ into blocks of size $\tilde{N}$
  for $\tilde{n} = 1 : \lfloor N + 1/\tilde{N} \rfloor$ **do**
    Denote block $\tilde{n}$ by $\mathbf{Y}_{\tilde{n}}$
    Estimate $\theta_{\tilde{n}}$ and $\delta_{\tilde{n}}$ from $\mathbf{Y}_{\tilde{n}}$ as in Section III-B
  end for
  Solve for $\mathbf{x}$:
$$\hat{\mathbf{x}} = \arg\min_{\mathbf{x}} \sum_{\tilde{n}=1}^{\lfloor N+1/\tilde{N} \rfloor} \frac{\left(\hat{\theta}_{\tilde{n}} - \arccos\left(\frac{x - \tilde{x}_{\tilde{n}}}{\|\mathbf{x} - \tilde{\mathbf{x}}_{\tilde{n}}\|}\right)\right)^2}{2\sigma_{\theta,\tilde{n}}^2}$$
  Solve for B:
$$\hat{B} = \arg\min_{B} \sum_{\tilde{n}=1}^{\lfloor N+1/\tilde{N} \rfloor} \frac{\left(\hat{\delta}_{\tilde{n}} - \|\hat{\mathbf{x}} - \tilde{\mathbf{x}}_{\tilde{n}}\| - B\right)\right)^2}{2\sigma_{\delta,\tilde{n}}^2}$$
  return $\hat{\mathbf{x}}, \hat{B}$
end procedure

The observation model in near-field is no longer of the form (13) so that a 2D-FFT will lead to multiple peaks. A pure maximum likelihood approach can be formulated, but leads to many local optima. Instead, we propose to extend the method from Section III-B with a simple sub-arrays approach as in [11], [18], without aiming for an optimal solution. We divide the array (equivalently, the rows of $\mathbf{Y}\mathbf{S}^{\mathrm{H}}(\mathbf{S}\mathbf{S}^{\mathrm{H}})^{-1}$) into non-overlapping sub-arrays with $\tilde{N}$ elements.[2] The value of $\tilde{N}$ should be chosen to satisfy the following conditions: (i) *far-field condition:* $\tilde{N} \leq \sqrt{\bar{d}\lambda}/(2\Delta^2)$, so that the far-field assumption is valid per sub-array (here, $\bar{d}$ is an expected distance to the UE); (ii) *narrowband condition:* $\tilde{N} \ll c/(W\Delta)$, so that paths are unresolved in the delay domain per sub-array. With these conditions (and ensuring that $\tilde{N} \geq 1$), the method from Section III-B can be applied to each sub-array, providing $\lfloor (N+1)/\tilde{N} \rfloor$ estimates

$$\hat{\theta}_{\tilde{n}} = \arccos\left(\frac{x - \tilde{x}_{\tilde{n}}}{\|\mathbf{x} - \tilde{\mathbf{x}}_{\tilde{n}}\|}\right) + w_{\theta,\tilde{n}}, \tag{17}$$

$$\hat{\delta}_{\tilde{n}} = \|\mathbf{x} - \tilde{\mathbf{x}}_{\tilde{n}}\| - B + w_{\delta,\tilde{n}}, \tag{18}$$

where $w_{\theta,\tilde{n}}$ and $w_{\delta,\tilde{n}}$ are measurement errors with variances $\sigma_{\theta,\tilde{n}}^2$ and $\sigma_{\delta,\tilde{n}}^2$, due to the background noise and the finite resolution of the FFTs. From these sub-array estimates, we can recover the UE position by intersecting the bearing lines and then the clock bias from the delay estimates. The complete procedure can be found in Algorithm 1. The complexity of

[2]Sub-array $\tilde{n}$ corresponding to the observations at antenna $(\tilde{n}-1)\tilde{N}+1$ through $\tilde{n}\tilde{N}$, with array center $\tilde{\mathbf{x}}_{\tilde{n}} = \mathbf{x}_{-N/2} + [\Delta((\tilde{n}-1)\tilde{N}+1+\tilde{N}/2,\, 0]^{\mathrm{T}}$. Here indexing $\tilde{n}$ starts at 1.

the method is of order $\mathcal{O}(NK \log \tilde{N}K)$. Note that in the narrowband far-field regime, $\tilde{N} = N + 1$, so that the method reverts to the one from Section III-B.

V. Numerical Results

We consider a nominal scenario at a carrier f_c of 28 GHz ($\lambda \approx 1.07$ cm), a bandwidth W of 100 MHz, $c = 0.3$ m/ns, $N_0 = 4.0049 \times 10^{-9}$ mW/GHz, a transmit power P_t of 1 mW (with $\mathbb{E}\{|s[k]|^2\} = P_t/W$) and $K + 1 = 257$ subcarriers with QPSK pilots. The UE has bias $B = 20$ m. The array has $N + 1 = 129$ elements spaced at $\lambda/2$, corresponding to a total size of 69.11 cm and a far-field distance of 89 m.[3]

A. Fisher Information

We will evaluate the position error bound (PEB[4]) for several models: the general (correct) model (1), and three approximate models: the standard model (3), the narrowband near-field model (15), and the spatial wideband far-field model (16), for known and unknown clock bias B. In Fig. 3 we show the PEB as as a function of the distance d. As expected, the far-field model is correct for distances larger than about 8 m, while for shorter distances the near-field models provide lower PEB. Moreover, at short distances, the PEB of the general model does not depend on whether we know B, while for large distances, the PEB quickly increases when B is unknown. The results clearly show that joint synchronization and positioning in near-field can give good performance.

In Fig. 4, we show the PEB as a function of the inter-antenna spacing. In this case, the PEB under the standard model does not depend on Δ, as it is mainly limited by the estimation of the distance. The general model leads to lower PEB for large antenna spacing, and larger PEB for small antenna spacing (for the case of unknown B). Note that for very large Δ, the PEB of the general model increases due to the path loss (antenna elements will be further away, reducing $|\alpha_n|$). For both figures, we see that the main benefit for small d or large Δ comes from the near-field information, not the spatial wideband information.

B. Algorithm

We now evaluate the performance of the method described in Section IV-C, whereby the AOAs are computed using a 2DFFT with $10N$ points in the spatial domain and $K + 1$ points in the frequency domain. We vary d with random $\theta \sim \mathcal{U}(\pi/4, 3\pi/4)$ and place a scatterer with radar cross section of 10 m^2 uniformly in the plane (this corresponds to a large scattering object). This enables us to evaluate the robustness to multipath. For comparison purposes, the method from Section III-B is also evaluated, assuming known bias. From Fig. 5, we observe low position RMSE for distances below 3 m. The non-LOS (NLOS) path increases the RMSE compared to the LOS-only case, as it causes large outliers. Note that multipath appears as a second peak in the 2D-FFT

[3]Source code is available at https://tinyurl.com/y3jybhdp.

[4]The PEB is defined from the 4×4 FIM $\mathbf{J}(\psi, \mathbf{x}, B)$ as $\sqrt{\text{trace}[\mathbf{J}^{-1}(\psi, \mathbf{x}, B)]_{2:3,2:3}}$ and is expressed in m.

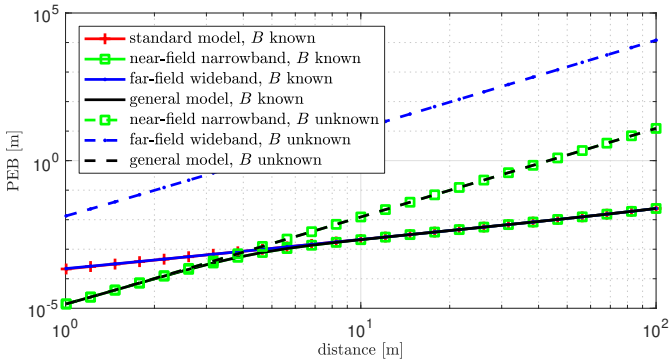

Fig. 3. PEB as a function of UE distance for known and unknown clock bias B, with $\Delta = \lambda/2$.

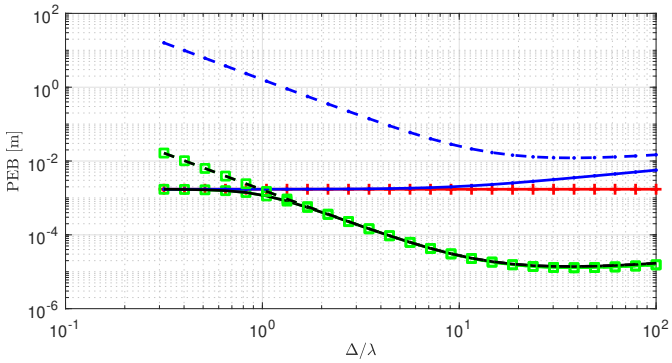

Fig. 4. PEB as a function of inter-antenna spacing for known and unknown clock bias B, with $\mathbf{x} = [1\,\text{m},\ 8\,\text{m}]^{\text{T}}$. The legend is the same as in Fig. 3.

and can thus be recovered and separated from the LOS path. However, which path corresponds to LOS is often harder to determine due to the poor delay resolution (the resolution at $W = 100$ MHz is only 3 m). Beyond 15 m distance, $\tilde{N} \to 1$, so that the problem is no longer identifiable. The localization performance is worse than the PEB from Fig. 3, as the method has not been optimized for accuracy. Moreover, the bias estimate has orders of magnitude larger error, as it is based on low-quality range estimates. This error can be further reduced by using larger FFTs along the frequency dimension. The far-field method from Section III-B with known bias is limited by the bandwidth and thus leads to worse performance for all d.

VI. Conclusions

When large arrays are used for positioning, near-field propagation must be taken into account. This presents challenges and opportunities for the development of localization systems beyond 5G. We have performed a Fisher information analysis and proposed a simple joint localization and synchronization method for this regime. Our results show that near-field propagation can be exploited in uplink and that the Fisher information provided from wavefront curvature is more pronounced than from spatial wideband. Immediate suggestions for future research are the inclusion of hybrid combining at

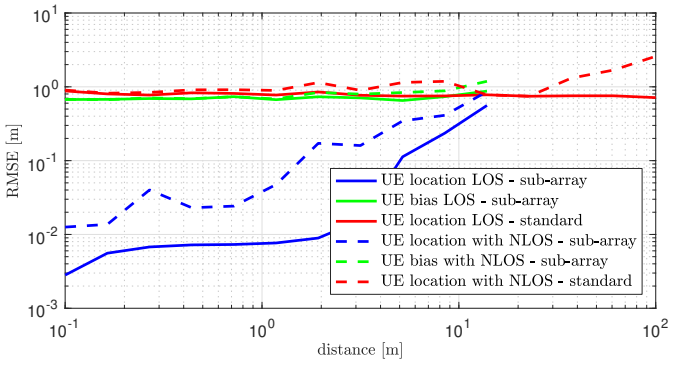

Fig. 5. Joint localization and synchronization performance using sub-array processing vs standard processing with LOS only and with multipath (LOS + NLOS). Bounds are not included, as they are loose since the algorithm is developed for proof-of-concept, not for ultimate accuracy.

the BS, as in [11], the study of downlink localization with a single receive antenna [29], as well as the inclusion of a more realistic propagation model [30], accounting for coupling [31] and electromagnetic theory, as well as jointly localizing and synchronizing multiple mobile users [25].

ACKNOWLEDGMENT

This research was supported, in part, by the Swedish Research Council under grant No. 2018-03701.

REFERENCES

[1] J. A. del Peral-Rosado, R. Raulefs, J. A. López-Salcedo, and G. Seco-Granados, "Survey of cellular mobile radio localization methods: From 1G to 5G," *IEEE Communications Surveys Tutorials*, vol. 20, pp. 1124–1148, Secondquarter 2018.

[2] H. Wymeersch, G. Seco-Granados, G. Destino, D. Dardari, and F. Tufvesson, "5G mm-Wave positioning for vehicular networks," *Wireless Commun. Mag.*, vol. 24, pp. 80–86, Dec. 2018.

[3] R. M. Buehrer, H. Wymeersch, and R. M. Vaghefi, "Collaborative sensor network localization: Algorithms and practical issues," *Proceedings of the IEEE*, vol. 106, no. 6, pp. 1089–1114, 2018.

[4] N. Garcia, H. Wymeersch, E. G. Larsson, A. M. Haimovich, and M. Coulon, "Direct localization for massive MIMO," *IEEE Transactions on Signal Processing*, vol. 65, no. 10, pp. 2475–2487, 2017.

[5] A. Shahmansoori, G. E. Garcia, G. Destino, G. Seco-Granados, and H. Wymeersch, "Position and orientation estimation through millimeter-wave MIMO in 5G systems," *IEEE Trans. Wireless Commun.*, vol. 17, pp. 1822–1835, Mar. 2018.

[6] Y. Han, Y. Shen, X.-P. Zhang, M. Z. Win, and H. Meng, "Performance limits and geometric properties of array localization," *IEEE Transactions on Information Theory*, vol. 62, no. 2, pp. 1054–1075, 2016.

[7] Y. Shen and M. Z. Win, "On the accuracy of localization systems using wideband antenna arrays," *IEEE Transactions on Communications*, vol. 58, no. 1, pp. 270–280, 2010.

[8] Y. Shen and M. Z. Win, "Fundamental limits of wideband localization – part I: A general framework," *IEEE Transactions on Information Theory*, vol. 56, pp. 4956–4980, 10 2010.

[9] K. Witrisal, P. Meissner, E. Leitinger, Y. Shen, C. Gustafson, F. Tufvesson, K. Haneda, D. Dardari, A. F. Molisch, A. Conti, *et al.*, "High-accuracy localization for assisted living: 5G systems will turn multipath channels from foe to friend," *IEEE Signal Processing Magazine*, vol. 33, no. 2, pp. 59–70, 2016.

[10] E. Björnson, L. Sanguinetti, H. Wymeersch, J. Hoydis, and T. L. Marzetta, "Massive mimo is a reality–what is next?: Five promising research directions for antenna arrays," *Digital Signal Processing*, 2019.

[11] N. J. Myers, J. Kaleva, A. Tölli, and R. W. Heath Jr, "Message passing-based link configuration in short range millimeter wave systems," *arXiv:1907.05009 [cs, eess, math]*, July 2019. arXiv: 1907.05009.

[12] E. Basar, M. Di Renzo, J. De Rosny, M. Debbah, M.-S. Alouini, and R. Zhang, "Wireless communications through reconfigurable intelligent surfaces," *IEEE Access*, vol. 7, pp. 116753–116773, 2019.

[13] S. Hu, F. Rusek, and O. Edfors, "Beyond Massive MIMO: The Potential of Positioning With Large Intelligent Surfaces," *IEEE Transactions on Signal Processing*, vol. 66, pp. 1761–1774, Apr. 2018.

[14] Y. Rockah and P. Schultheiss, "Array shape calibration using sources in unknown locations–part ii: Near-field sources and estimator implementation," *IEEE Transactions on Acoustics, Speech, and Signal Processing*, vol. 35, no. 6, pp. 724–735, 1987.

[15] Y.-D. Huang and M. Barkat, "Near-field multiple source localization by passive sensor array," *IEEE Transactions on antennas and propagation*, vol. 39, no. 7, pp. 968–975, 1991.

[16] N. Yuen and B. Friedlander, "Performance analysis of higher order ESPRIT for localization of near-field sources," *IEEE Transactions on Signal Processing*, vol. 46, pp. 709–719, Mar. 1998.

[17] H. Gazzah and J. P. Delmas, "CRB-based design of linear antenna arrays for near-field source localization," *IEEE Transactions on Antennas and Propagation*, vol. 62, no. 4, pp. 1965–1974, 2014.

[18] W. Zhi and M. Y. Chia, "Near-field source localization via symmetric subarrays," *IEEE Signal Processing Letters*, vol. 14, pp. 409–412, June 2007.

[19] M. N. El Korso, R. Boyer, A. Renaux, and S. Marcos, "Conditional and unconditional Cramér–Rao bounds for near-field source localization," *IEEE Transactions on Signal Processing*, vol. 58, no. 5, pp. 2901–2907, 2010.

[20] K. Hu, S. P. Chepuri, and G. Leus, "Near-field source localization: Sparse recovery techniques and grid matching," in *2014 IEEE 8th Sensor Array and Multichannel Signal Processing Workshop (SAM)*, pp. 369–372, IEEE, 2014.

[21] W. Zuo, J. Xin, N. Zheng, and A. Sano, "Subspace-based localization of far-field and near-field signals without eigendecomposition," *IEEE Transactions on Signal Processing*, vol. 66, no. 17, pp. 4461–4476, 2018.

[22] S. Zhang, T. Jost, R. Pöhlmann, A. Dammann, D. Shutin, and P. A. Hoeher, "Spherical wave positioning based on curvature of arrival by an antenna array," *IEEE Wireless Communications Letters*, vol. 8, pp. 504–507, April 2019.

[23] J. Chen, R. Hudson, and Kung Yao, "Maximum-likelihood source localization and unknown sensor location estimation for wideband signals in the near-field," *IEEE Transactions on Signal Processing*, vol. 50, pp. 1843–1854, Aug. 2002.

[24] K. Mada, Hsiao-Chun Wu, and S. Iyengar, "Efficient and Robust EM Algorithm for Multiple Wideband Source Localization," *IEEE Transactions on Vehicular Technology*, vol. 58, pp. 3071–3075, July 2009.

[25] M. Z. Win, Y. Shen, and W. Dai, "A theoretical foundation of network localization and navigation," *Proceedings of the IEEE*, vol. 106, no. 7, pp. 1136–1165, 2018.

[26] D. Dardari, A. Conti, U. Ferner, A. Giorgetti, and M. Z. Win, "Ranging with ultrawide bandwidth signals in multipath environments," *Proceedings of the IEEE*, vol. 97, pp. 404–426, Feb 2009.

[27] S. Kay, *Fundamentals of Statistical Signal Processing: Estimation Theory*. Prentice Hall Signal Processing Series, 1993.

[28] F. Rusek, D. Persson, B. K. Lau, E. G. Larsson, T. L. Marzetta, O. Edfors, and F. Tufvesson, "Scaling Up MIMO: Opportunities and Challenges with Very Large Arrays," *IEEE Signal Processing Magazine*, vol. 30, pp. 40–60, Jan. 2013.

[29] A. Fascista, A. Coluccia, H. Wymeersch, and G. Seco-Granados, "Millimeter-wave downlink positioning with a single-antenna receiver," *IEEE Transactions on Wireless Communications*, pp. 1–1, 2019.

[30] B. Friedlander, "Localization of signals in the near-field of an antenna array," *IEEE Transactions on Signal Processing*, vol. 67, pp. 3885–3893, Aug 2019.

[31] T. Svantesson, *Antennas and propagation from a signal processing perspective*. PhD thesis, Chalmers University of Technology, Sweden, 2001.